AIAA JOURNAL
Vol. 39, No. 6, June 2001

Aeroacoustic Modeling of Turbulent Airfoil Flows

Wen Zhong Shen* and Jens Nørkær Sørensen†
Technical University of Denmark, DK-2800 Lyngby, Denmark

A numerical algorithm for acoustic noise generation is extended to handle turbulent flows. The approach involves two steps comprising a viscous incompressible flow part and an inviscid acoustic part. In the turbulent case, the flow is further split into a Reynolds-averaged component and a component corresponding to the turbulent small-scale fluctuations. The latter is modeled by an eddy-viscosity-based turbulence model and appears as a source term in the acoustic equations. The formulation is applied to acoustic noise generated by the flow past a NACA 0015 airfoil at an incidence of 20 deg. First, acoustic noise generated by laminar flow is considered as a validation of the acoustic model. The results are compared to solutions obtained using the Lighthill acoustic analogy (linearized wave equations) (Lighthill, M. J., "On Sound Generated Aerodynamically. I: General Theory," *Proceedings of the Royal Society of London, Series A: Mathematical and Physical Sciences*, Vol. 211, 1952, pp. 564–587). The comparisons show that noise levels and frequency content are in good agreement. Next, the acoustic model is applied on a turbulent flow in which the small-scale turbulence is modeled by a Reynolds-averaged turbulence model [Baldwin–Barth one equation model (Baldwin, B. S., and Barth, T. J., "A One-Equation Turbulence Transport Model for High Reynolds Number Wall-Bounded Flows," NASA TM 102847, 1990)]. The computations show that the generated acoustic field is dominated by the Strouhal frequency and its harmonics. The acoustic noise level for the turbulent flow is of the same order as for the laminar flow. Because of the turbulence model used in the flow solver, only one frequency and its higher harmonics are seen. For capturing more frequencies, one should combine the acoustic model with large eddy simulation or direct Navier–Stokes simulation.

Nomenclature

C_d	=	drag coefficient
C_l	=	lift coefficient
k	=	turbulent kinetic energy
M	=	Mach number
$\bar{P}$	=	mean/filtered incompressible pressure
p	=	pressure
p_0	=	ambient pressure
$\bar{p}$	=	$\bar{P} + p^*$
p^*	=	acoustic pressure
$\bar{p}^*$	=	mean/filtered acoustic pressure
$p^{*\prime}$	=	turbulent acoustic pressure
Re	=	Reynolds number
r	=	distance from the airfoil center
t	=	time
$\bar{U}_i$	=	ith mean/filtered incompressible velocity component
U_i'	=	ith turbulent fluctuating incompressible velocity component
u_i	=	ith velocity component
u_i^*	=	ith acoustic velocity component
$\bar{u}_i^*$	=	ith mean/filtered acoustic velocity component
$u_i^{*\prime}$	=	ith turbulent acoustic velocity component
x_i	=	ith coordinate
ν	=	kinematic viscosity
ν_t	=	eddy viscosity
ρ	=	density
ρ_0	=	ambient density
ρ^*	=	acoustic density
$\bar{\rho}^*$	=	mean/filtered acoustic density
$\rho^{*\prime}$	=	turbulent acoustic density
ψ	=	incompressible stream function
ω	=	incompressible vorticity

Received 18 February 2000; revision received 10 October 2000; accepted for publication 25 October 2000.

*Associate Professor, Department of Energy Engineering, Building 403; also Associate Professor, Research Center for High Speed Trains, Changsha Railway University, Hunan 410075, People's Republic of China.

†Associate Professor, Department of Energy Engineering, Building 403.

I. Introduction

IT has long been recognized that there is an increasing need for predicting aerodynamically generated noise from flows, such as helicopter, wind turbine, and jet flows. Common for most aerodynamic noise prediction codes in use today is that they are based on the Lighthill acoustic analogy[1] resulting in linearized wave equations combined with sound sources, such as monopoles, dipoles, and quadrupoles.[2,3] Recently, Hardin and Pope[4] proposed a nonlinear two-step procedure for computational aeroacoustics that is suitable for both generation and propagation. In this approach, the viscous flow is obtained from the incompressible Navier–Stokes equations and a correction to the constant hydrodynamic density is defined. Once this is defined, the acoustic radiation is obtained from the numerical solution of a system of perturbed, compressible inviscid equations. The advantage of the splitting approach, as compared to the acoustic analogy theories, is that the source strength is obtained directly and that it accounts for sound radiation as well as scattering. Based on the pioneering work of Hardin and Pope, a general aeroacoustic model was recently developed by the authors.[5] This new formulation was previously applied to laminar flows around a circular cylinder.[6]

For airflows in most industrial applications, the flowfield is complex and turbulent. The idea of the paper is to develop further the acoustic formulation to simulate noise generated by turbulent flows.

The paper is organized as follows. In Sec. II, the governing equations and hypotheses are discussed, followed by a set of acoustic equations for both laminar and turbulent flows. The numerical implementation is given in Sec. III. Results are presented for both laminar and turbulent flows in Sec. IV.

II. Formulation of the Problem

Based on the splitting approach introduced by Hardin and Pope,[4] a numerical algorithm for acoustic noise generation was developed by Shen and Sørensen.[6] The algorithm consists of two steps comprising a viscous incompressible flow part and an inviscid acoustic part. The model is suitable for both generation and propagation of aeroacoustic noise and has previously been applied to analyze aeroacoustic noise generated from laminar flows past a cylinder. In this section, we will show how the model may be further developed to deal with turbulent flows by using an eddy-viscosity-based turbulence model.

A. Decomposition of Variables

The main idea of the splitting approach is to decompose each of the variables into an incompressible component and an acoustic one. In the turbulent case, the variables are further decomposed into Reynolds-averaged and fluctuating components. Exemplified by a general variable f, the decomposition reads

$$f = F + f^* = \bar{F} + F' + \bar{f}^* + f^{*\prime} \tag{1}$$

where the incompressible component is denoted by a capital letter and an asterisk designates the acoustic component.

The fluctuating terms are due to small-scale turbulence that is characterized by a timescale τ. In the following, it is assumed that the turbulent fluctuations of the acoustic field is negligible; hence, $f^{*\prime} \approx 0$. Reynolds averaging is taken over a time interval T_r such that

$$\bar{F} = \frac{1}{T_r}\int_{t_0}^{t_0+T_r} F\,\mathrm{d}t \tag{2}$$

$$\bar{f}^* = \frac{1}{T_r}\int_{t_0}^{t_0+T_r} f^*\,\mathrm{d}t \tag{3}$$

where $\tau \ll T_r \ll T$, with T a characteristic timescale for large-scale fluctuations due to vortex shedding. The decomposition is shown in Fig. 1.

Because we expect the large-scale fluctuations to be periodic, a time-averaged flowfield is defined as

$$\tilde{f} = \frac{1}{nT}\int_{t_0}^{t_0+nT} f\,\mathrm{d}t \tag{4}$$

where n is an integer defining the number of periods over which the averaging is performed.

As discussed in detail by Shen and Sørensen,[6] the principle behind the splitting technique is to introduce the decomposition of Eq. (1) into the compressible flow equations and to subtract the incompressible Navier–Stokes equations from these. This results in a set of acoustic equations in which the time derivative of the incompressible pressure acts as a source term. In the turbulent case, the procedure is essentially the same except that the decomposition is carried out for the Reynolds-averaged equations. This involves Reynolds averaging of the nonlinear convective terms. For the two general variables f and g, this gives

$$\overline{fg} = \overline{(\bar{F} + F' + \bar{f}^*)(\bar{G} + G' + \bar{g}^*)} \tag{5}$$

$$\overline{fg} = \bar{F}\bar{G} + \overline{F'G'} + \bar{F}\bar{g}^* + \bar{f}^*\bar{G} + \bar{f}^*\bar{g}^* \tag{6}$$

where $\overline{F'G'}$ is a Reynolds stress, modeled by an eddy-viscosity hypothesis. Both $\bar{F}\bar{G}$ and $\overline{F'G'}$ are determined from a solution of the incompressible Navier–Stokes equations. When the incompressible flow components $\bar{F}$ and $\bar{G}$ have been determined, the remaining three terms that appear in the acoustic equations are subsequently solved for the acoustic variables $\bar{f}^*$ and $\bar{g}^*$.

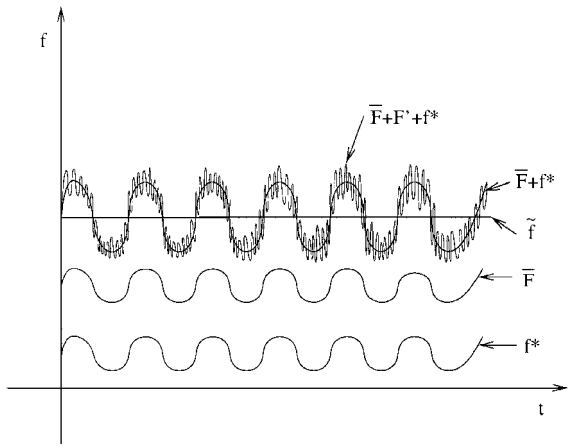

Fig. 1 Decomposition of f into Reynolds-averaged components, $\bar{F}$ (incompressible) and $\bar{f}^*$ (acoustic), and a fluctuating incompressible component F'.

B. Flow Equations

Because the work reported here concerns flows at small Mach numbers ($M \leq 0.3$), we employ an incompressible solver for the flow equations. In principle, a compressible solution algorithm may be utilized to compute flows at all Mach numbers. At small Mach numbers, however, the speed of sound restricts the size of the time step so much that the computing costs become prohibitive. In primitive variables, the Reynolds-averaged [or filtered for large-eddy simulation (LES)] incompressible Navier–Stokes equations read

$$\frac{\partial \bar{U}_i}{\partial t} + \frac{\partial(\bar{U}_i\bar{U}_j)}{\partial x_j} = -\frac{1}{\rho_0}\frac{\partial \bar{P}}{\partial x_i} + \nu\frac{\partial^2 \bar{U}_i}{\partial x_j^2} - \frac{\partial(\overline{U_iU_j} - \bar{U}_i\bar{U}_j)}{\partial x_j} \tag{7}$$

$$\frac{\partial \bar{U}_i}{\partial x_i} = 0 \tag{8}$$

where $\bar{(\ )}$ denotes the average for Reynolds-averaged Navier–Stokes (RANS) or filtering for LES and the velocity is decomposed into a mean/filtered component $\bar{U}_i$ and a turbulent fluctuating component U_i', that is, $U_i = \bar{U}_i + U_i'$.

For RANS, the terms, $\overline{U_iU_j} - \bar{U}_i\bar{U}_j = \overline{U_i'U_j'}$, are referred to as the Reynolds stresses.

For LES, the subgrid stresses $\overline{U_iU_j} - \bar{U}_i\bar{U}_j$ can be decomposed as $(\overline{\bar{U}_i\bar{U}_j} - \bar{U}_i\bar{U}_j) + (\overline{\bar{U}_iU_j'} + \overline{U_i'\bar{U}_j}) + \overline{U_i'U_j'}$. The first term (the Leonard term) and second term (the cross term) are small and are usually neglected.

Using the Boussinesq approximation, the Reynolds stresses are modeled by introducing an eddy viscosity ν_t:

$$-\overline{U_i'U_j'} = \nu_t\left(\frac{\partial \bar{U}_i}{\partial x_j} + \frac{\partial \bar{U}_j}{\partial x_i}\right) - \frac{2}{3}k\delta_{ij} \tag{9}$$

Then the final incompressible flow equations become

$$\frac{\partial \bar{U}_i}{\partial t} + \frac{\partial(\bar{U}_i\bar{U}_j)}{\partial x_j} = -\frac{1}{\rho_0}\frac{\partial(\bar{P} + 2/3\rho_0 k)}{\partial x_i} + \frac{\partial}{\partial x_j}\left[(\nu + \nu_t)\left(\frac{\partial \bar{U}_i}{\partial x_j} + \frac{\partial \bar{U}_j}{\partial x_i}\right)\right] \tag{10}$$

$$\frac{\partial \bar{U}_i}{\partial x_i} = 0 \tag{11}$$

Solving the Reynolds-averaged equations by a time-true integration procedure is sometimes referred to as VLES (very large eddy simulation). The reason for choosing Reynolds averaging instead of LES filtering, is that the latter in the two-dimensional case results in unphysical solutions such as inverse cascade phenomena for the higher frequencies in the inertial subrange. In the present case, the small-scale fluctuations are modeled as if they were three-dimensional, whereas intrinsic two-dimensional behavior only exists for the lower frequencies associated with vortex shedding.

In the present case only two-dimensional flows are considered, and the equivalent stream function-vorticity ($\psi - \omega$) form is used. Details about the formulation and the numerical algorithm may be found in Ref. 7.

C. Acoustic Equations

We now consider the acoustic equations. The basic formulation is based on the following decomposition of the compressible solution:

$$u_i = U_i + u_i^* = \bar{U}_i + U_i' + \bar{u}_i^* \tag{12}$$

$$p = P + p^* = \bar{P} + P' + \bar{p}^* \tag{13}$$

$$\rho = \rho_0 + \rho^* = \rho_0 + \bar{\rho}^* \tag{14}$$

where U_i is the incompressible velocity. When the decomposed variables are introduced into the compressible Navier–Stokes equations, the final acoustic equations are obtained. Details about the formulation for laminar acoustic noise may be found in Refs. 5 and 6.

For turbulent flows, when a turbulence model is used along with the RANS equations, the only available information from the incompressible solver is the instantaneous Reynolds-averaged solution. Our intention here is to study the noise generated by the main flow, not the small-scale turbulent fluctuations. Hence, the acoustic length scale and timescales analyzed are much larger than the turbulent ones, implying that the turbulent fluctuations of the acoustic field are small.

The Reynolds-averaged transformed acoustic variables $f_i = \rho u_i^* + \rho^* U_i$ are written as

$$\bar{f}_i = \overline{\rho u_i^* + \rho^* U_i} \tag{15}$$

$$\bar{f}_i = \bar{\rho}\bar{u}_i^* + \bar{\rho}^* \bar{U}_i \tag{16}$$

$$\bar{f}_i = \rho u_i^* + \rho^* \bar{U}_i \tag{17}$$

When the Reynolds-average of the f_i equation is taken, the convection term becomes

$$\overline{f_i\left(U_j + u_j^*\right)} = \overline{\left(\rho u_i^* + \rho^* U_i\right)\left(U_j + u_j^*\right)} \tag{18}$$

$$\overline{f_i\left(U_j + u_j^*\right)} = \overline{\rho u_i^*\left(U_j + u_j^*\right)} + \overline{\rho^* U_i U_j} + \overline{\rho^* U_i u_j^*} \tag{19}$$

$$\overline{f_i\left(U_j + u_j^*\right)} = \rho u_i^*\left(\bar{U}_j + u_j^*\right) + \rho^* \overline{U_i U_j} + \rho^* \bar{U}_i u_j^* \tag{20}$$

$$\overline{f_i\left(U_j + u_j^*\right)} = \bar{f}_i\left(\bar{U}_j + u_j^*\right) + \rho^*\left(\overline{U_i U_j} - \bar{U}_i \bar{U}_j\right) \tag{21}$$

where the last term is determined from Eq. (9).

For notation simplicity, we omit $\bar{\ }$ for the acoustic variables. Then the Reynolds-averaged acoustic equations for turbulent flows read

$$\frac{\partial \rho^*}{\partial t} + \frac{\partial f_i}{\partial x_i} = 0 \tag{22}$$

$$\frac{\partial f_i}{\partial t} + \frac{\partial}{\partial x_j}\left[f_i\left(\bar{U}_j + u_j^*\right) + \rho_0 \bar{U}_i u_j^* + \left(p^* + \tfrac{2}{3}\rho^* k\right)\delta_{ij}\right]$$

$$= \frac{\partial}{\partial x_j}\left[\rho^* \nu_t\left(\frac{\partial \bar{U}_i}{\partial x_j} + \frac{\partial \bar{U}_j}{\partial x_i}\right)\right] \tag{23}$$

$$\frac{\partial p^*}{\partial t} - c^2 \frac{\partial \rho^*}{\partial t} = -\frac{\partial \bar{P}}{\partial t} \tag{24}$$

where now $f_i = \rho u_i^* + \rho^* \bar{U}_i$ and $c^2 = \gamma(\bar{P} + p^*)/(\rho_0 + \rho^*)$.

As compared to the laminar acoustic formulation, the additional terms, $\partial(\frac{2}{3}\rho^* k)/\partial x_i$ and $\partial/\partial x_j[\rho^* \nu_t(\partial \bar{U}_i/\partial x_j + \partial \bar{U}_j/\partial x_i)]$, appear in the acoustic velocity equations. These terms are considered as additional acoustic source terms associated with the Reynolds stresses of the turbulent flow.

III. Turbulence Model

The turbulence model used in this paper is the one-equation model of Baldwin and Barth,[8] which in earlier works has shown to give good results for airfoils subject to stall (see Sørensen[9]).

To run the acoustic equations, we need to compute the turbulent kinetic energy k. In the model of Baldwin and Barth,[8] k is not given explicitly. To compute k, the dominant part of k, however, can be obtained as $\sqrt{(\nu\tilde{R}_T P)}$, where $\nu\tilde{R}_T$ is the equation variable and P, which is the production of k, is computed when solving the $\nu\tilde{R}_T$ equation.

IV. Numerical Discretization of the Acoustic Equations

We discuss briefly the numerical discretization of the acoustic equations (22–24). The discretizations of both the incompressible and the acoustic equations are second-order accurate in time and space, $\mathcal{O}(\delta t^2, \delta x^2)$. More details about the discretization may be found in Refs. 6 and 7.

A. Temporal Discretization

To obtain a good resolution of Eqs. (22–24), it is preferable to stagger the variables in time, such that ρ^* and p^* are defined at time level $(n - \frac{1}{2})\delta t$ and the velocity components at time level $n\delta t$. The velocity equation (23) is discretized at time level $(n + \frac{1}{2})\delta t$ using a semi-implicit Adams–Bashforth/Crank–Nicolson scheme. The density equation (22) and the pressure equation (24) are written at time level $n\delta t$. The turbulent source terms appearing in the acoustic velocity equations are determined explicitly from the incompressible computations.

B. Spatial Discretization

The computational grid is generated by using a conformal mapping.[7] The transformed plane $[0, R_\xi] \times [0, 2]$ is divided into a $N_\xi \times N_\eta$ regular mesh, with spatial mesh sizes $\delta\xi = R_\xi/(N_\xi - 1)$ and $\delta\eta = 2/(N_\eta - 1)$.

Because the acoustic equations are inviscid, the only boundary condition is the slip condition ($\boldsymbol{u} \cdot \boldsymbol{n} = 0$). For this kind of problem it is of advantage to use a staggered grid. The derivatives are discretized by a standard second-order centered difference scheme, with the exception of the convective–deformative terms in the acoustic velocity equations that are discretized by the second-order upwind QUICK scheme.

The turbulent source terms are determined on the acoustic grid after interpolating the modeled incompressible Reynolds stresses $\nu_t(\partial \bar{U}_i/\partial x_j + \partial \bar{U}_j/\partial x_i)$ and the turbulent kinetic energy k from the incompressible mesh to the acoustic grid.

V. Numerical Results and Discussion

The method is applied for laminar and turbulent flows past a NACA 0015 airfoil at 20-deg incidence and Mach number $M = 0.2$.

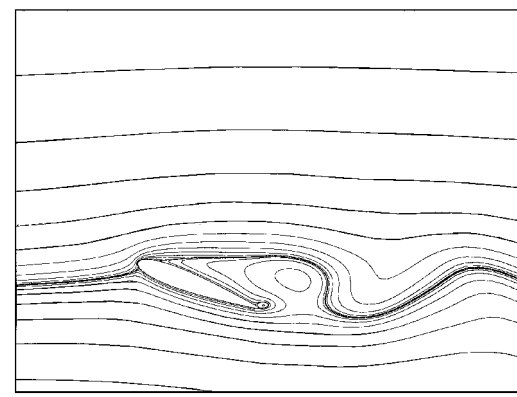

Fig. 2 Streamline plot of flow past a NACA 0015 airfoil at *Re* = 300 and 20-deg incidence.

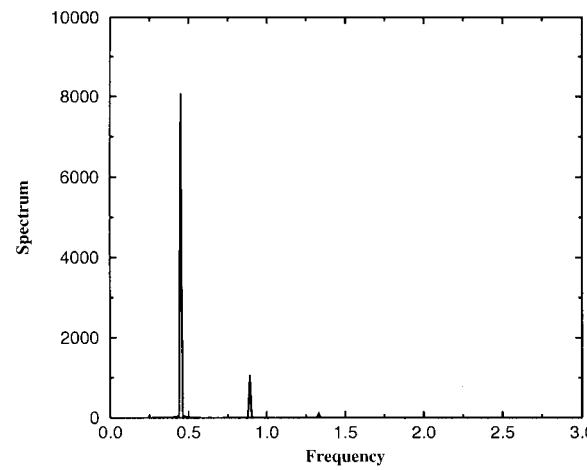

Fig. 3 Spectrum of the incompressible vorticity signal for laminar flow past a NACA 0015 airfoil at *Re* = 300 and 20-deg incidence.

A. Laminar Flow

To analyze the acoustic waves generated by vortex shedding, a laminar flow past a NACA 0015 airfoil at $Re = 300$, 20-deg incidence, and $M = 0.2$ is computed. The incompressible solution is calculated on a 121×161 O grid generated by conformal mapping in a domain of radius equal to about 25 chord lengths. The acoustic solution is performed on an O grid consisting of 61×81 grid points in the same domain. After a nondimensional time of $t = 40$, the incompressible periodic state is established, and the acoustic computation is started.

The streamlines of the incompressible solution are plotted in Fig. 2. The time-dependent vorticity signal at a point downstream

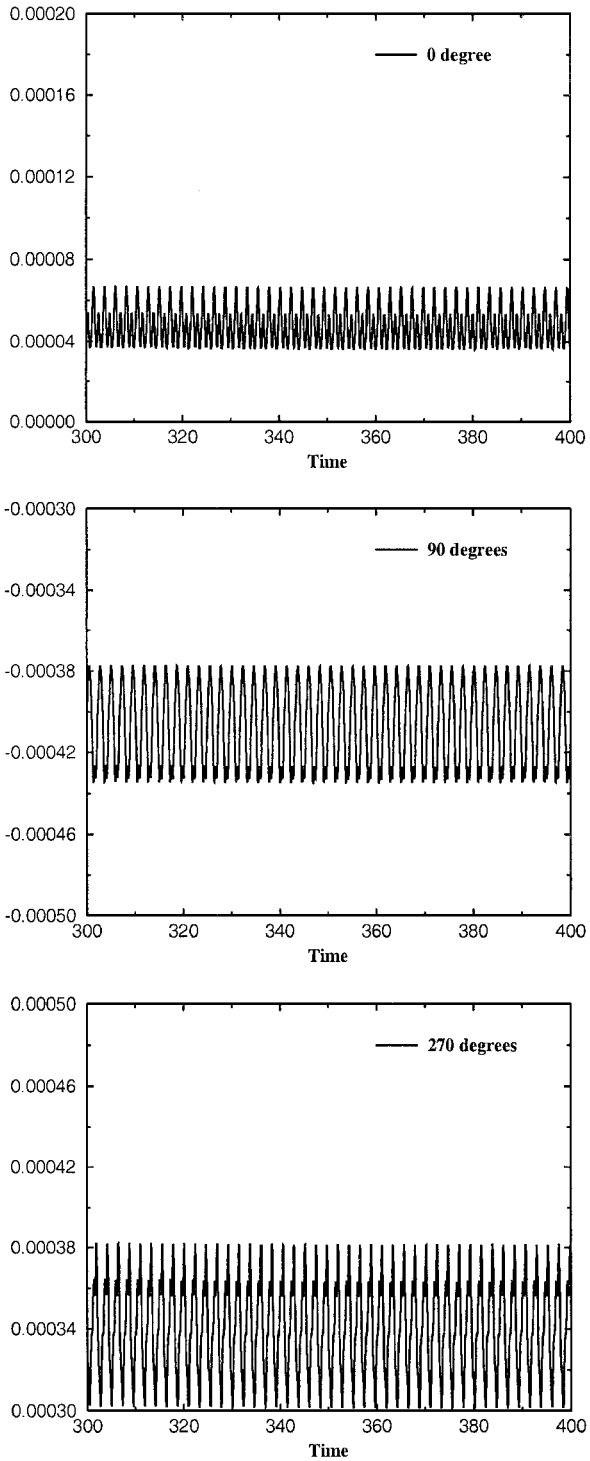

Fig. 4 Normalized pressure $(p - p_0)/p_0$ at $r = 12$ for laminar flow past a NACA 0015 airfoil at $Re = 300$, 20-deg incidence, and $M = 0.2$, measured at three points around the airfoil.

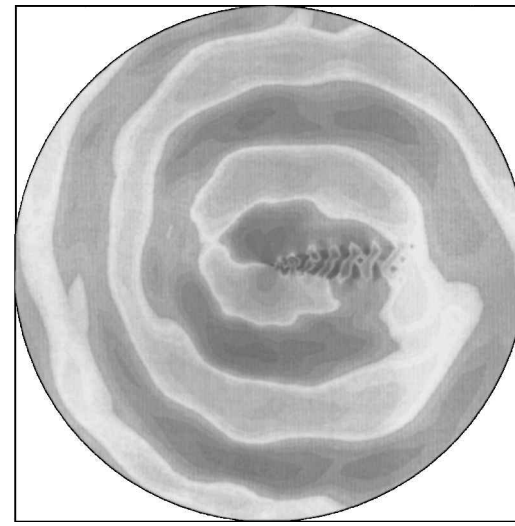

Fig. 5 Instantaneous plot of fluctuating pressure, $\tilde{p} - \bar{p}$, for laminar flow past a NACA 0015 airfoil at $Re = 300$, 20-deg incidence, $M = 0.2$, and $t = 400$.

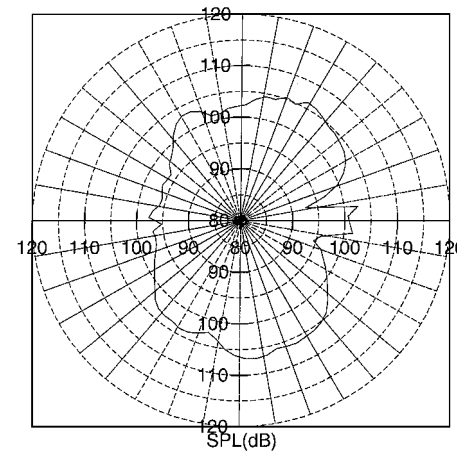

Fig. 6 Directivity pattern of NACA 0015 airfoil noise radiation at $Re = 300$, 20-deg incidence 20, $M = 0.2$, and $r = 12$.

near the trailing edge is stored. When performing fast Fourier transform (FFT) analysis, the power spectrum of the vorticity signal is obtained (Fig. 3). From Fig. 3, we get a vortex shedding Strouhal frequency equal to 0.452. Figure 4 shows time histories of the normalized pressure $(p - p_0)/p_0$ at $(x_1, x_2) = (12, 0)$, $(0, 12)$, and $(0, -12)$. The signals are seen to be dominated by the Strouhal frequency.

Because the pressure field is periodic and different from zero, a time-averaged pressure $\tilde{p}$ is defined from Eq. (4). In Fig. 5, a fluctuating pressure field $(p - \tilde{p})$ is plotted at time instant $t = 400$. As expected, the acoustic noise is mainly propagated in the direction normal to the freestream velocity. The fluctuating structures in the wake reveal the occurrence of source terms connected with vortex shedding. From Fig. 5, the number of acoustic waves is about 2.5 in the normal direction, which corresponds to about 24 grid points per wavelength. The directivity pattern of the airfoil noise radiation at $M = 0.2$, measured at a distance $r = 12$ from the airfoil center, is shown in Fig. 6. The levels range from 95 to 105 dB with a reference of 2×10^{-5} Pa. The directivity pattern is seen to be slightly asymmetric due to the finite incidence. In the wake a peak value appears, corresponding to the wave generated from the shed vorticity.

B. Validation of the Acoustic Algorithm

Before proceeding to the turbulent case, we perform a validation study of the acoustic algorithm.

A study on the numerical error introduced by the interpolation from the incompressible mesh to the acoustic mesh is carried out.

On the acoustic mesh, the incompressible velocity may be computed in two different ways: 1) direct interpolation from the velocity on the incompressible mesh or 2) direct interpolation of the stream function ψ and subsequent calculation of the velocity on the acoustic mesh.

When time histories of the pressure at an arbitrarily chosen monitor point $(x_1, x_2) = (0, 12)$ were compared, the same basic frequencies were obtained from the two interpolation techniques. The main difference was a slight change in the averaged level. Thus, the influence of the interpolation technique when going from the incompressible mesh to the acoustic mesh was found to be insignificant.

To analyze the sensitivity of the grid spacing, two additional computations were carried out. First, the number of grid points in the radial direction was increased from 61 to 101 for the direct velocity interpolation case. In Fig. 7, the time history of the normalized pressure is shown. From Fig. 7, the difference is seen to be small, except that increasing the number of points in radial direction tends to reduce the superharmonic frequencies. Next, the number of grid points in the tangential direction is doubled for the ψ interpolation case. From the time history shown in Fig. 8, the difference is also found to be small. Consequently, the solution is almost grid independent, and it is found to be sufficient to perform the computations on the 61×81 grid.

As a final validation of the algorithm, a comparative computation using the acoustic analogy based on the Ffowcs Williams–Hawkings equations[2] was carried out. In this approach, the acoustic pressure is expressed in monopole, dipole and quadrupole noise.[10,11] In the laminar case, the quadrupole noise is much smaller than the dipole noise and is not considered here. The acoustic pressures due to monopoles $p_m^*(\boldsymbol{x}, t)$ and dipoles $p_d^*(\boldsymbol{x}, t)$, respectively, are given as

$$4\pi p_m^*(\boldsymbol{x}, t) = \int_{f=0} \left[\frac{\rho_0(\dot{v}_n + v_{\dot{n}})}{r(1 - M_r)^2} \right]_{\text{ret}} \mathrm{d}S + \int_{f=0} \left\{ \frac{\rho_0 v_n \left[r\dot{M}_r + c\left(M_r - M^2\right) \right]}{r^2(1 - M_r)^3} \right\}_{\text{ret}} \mathrm{d}S \tag{25}$$

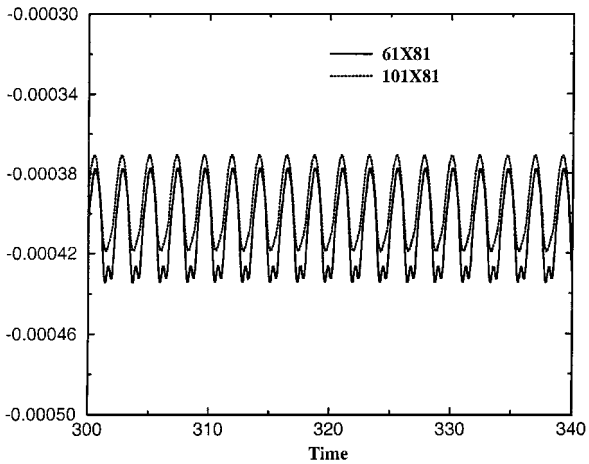

Fig. 7 Grid analysis for laminar flow past a NACA 0015 airfoil at $Re = 300$, 20-deg incidence, and $M = 0.2$.

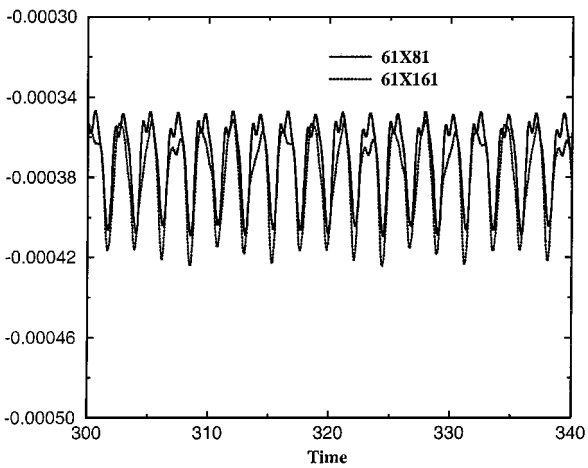

Fig. 8 Grid analysis for laminar flow past a NACA 0015 airfoil at $Re = 300$, 20-deg incidence, and $M = 0.2$.

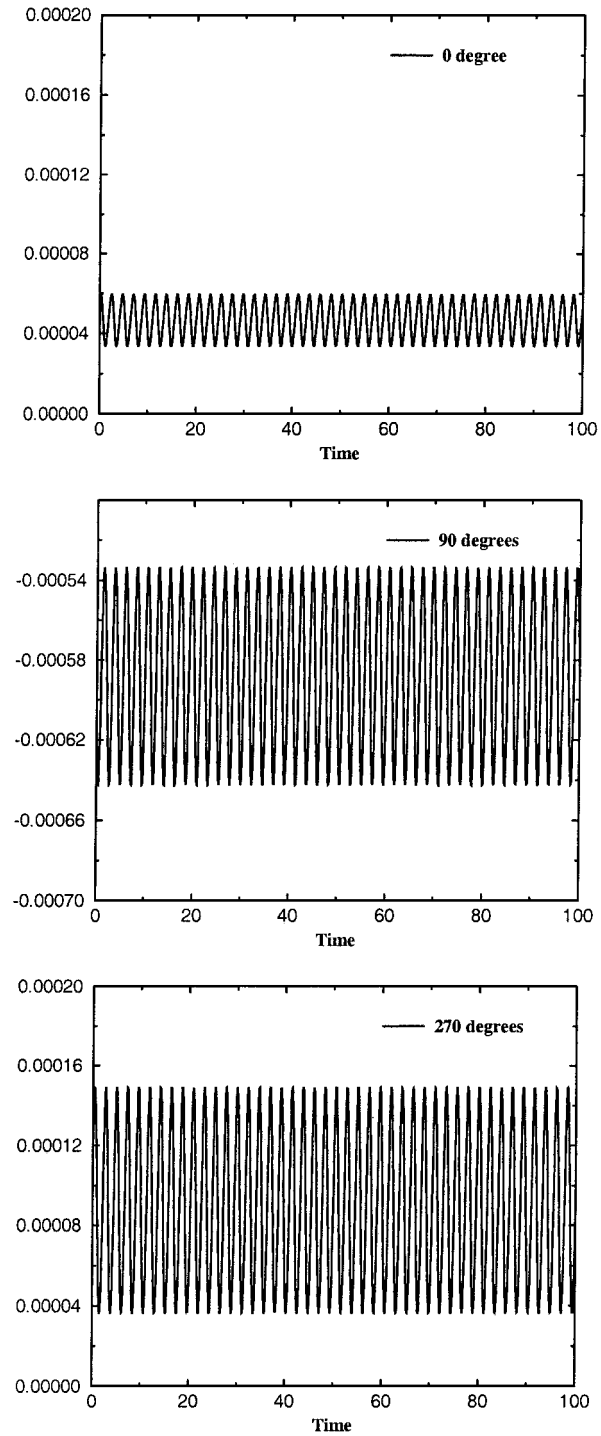

Fig. 9 Normalized pressure $(p - p_0)/p_0$ using the acoustic analogy; noise prediction at $r = 12$ for laminar flow past a NACA 0015 airfoil at $Re = 300$, 20-deg incidence, and $M = 0.2$, measured at three points around the airfoil.

$$4\pi p_d^*(\boldsymbol{x},t)=\frac{1}{c}\int_{f=0}\left[\frac{\dot{l}_r}{r(1-M_r)^2}\right]_{\text{ret}}\mathrm{d}S+\int_{f=0}\left[\frac{l_r-l_M}{r^2(1-M_r)^2}\right]_{\text{ret}}\mathrm{d}S+\frac{1}{c}\int_{f=0}\left\{\frac{l_r\left[r\dot{M}_r+c\left(M_r-M^2\right)\right]}{r^2(1-M_r)^3}\right\}_{\text{ret}}\mathrm{d}S \tag{26}$$

where v_n is the local velocity normal to the surface, l is the force per unit area acting on the fluid, M is the velocity of the body divided by the freestream sound speed c, and r is the distance from the observer position $\boldsymbol{x}$ to the source position $\boldsymbol{y}$. The subscripts r and n indicate a dot product of the considered vector with unit vectors in the direction of radiation and surface normal, respectively. Here, $v_{\dot{n}}$ is $v_i\,\partial n_i/\partial\tau$, where τ is the source time. The subscript ret indicates that the integrand is evaluated at the retarded time, and $f=0$ is the body surface.

In Fig. 9, time histories of the normalized pressure are shown at $(x_1, x_2)=(12, 0)$, $(0, 12)$, and $(0, -12)$. As compared to Fig. 4, the amplitudes (noise levels) are found to be of the same order, but slightly overpredicted. The same tendencies were observed by Cox et al.,[12] who computed the circular cylinder noise by the monopole and dipole approach and compared it to experimental data. The pressure levels are almost the same at the 0-deg position but smaller at 90- and 270-deg positions. Note, however, that the pressure level is not interesting in general acoustic noise computations.

C. Turbulent Flow

To study noise propagation from a turbulent flow, a NACA 0015 airfoil at $Re=1.5\times10^6$, 20-deg incidence, and $M=0.2$ is computed using the Baldwin–Barth turbulence model.[8] The incompressible solution is calculated on a 121×161 O grid generated by a conformal mapping in a domain of radius equal to about 25 chord lengths. To ensure that the first grid point off the airfoil surface is located at y^+ values less than 4, the height of the first computational cell is put equal to about 3×10^{-5}. The incompressible code has been validated for turbulent airfoil flows by Shen and Sørensen.[7] The acoustic solution is performed on an O grid consisting of 101×81 grid points in the same domain. After a nondimensional time of $t=40$, the incompressible periodic state is established, and the acoustic computation is started.

The streamlines of the incompressible solution for the turbulent flow are plotted in Fig. 10. When compared with the corresponding laminar flow case (see Fig. 2), the separation points are observed to

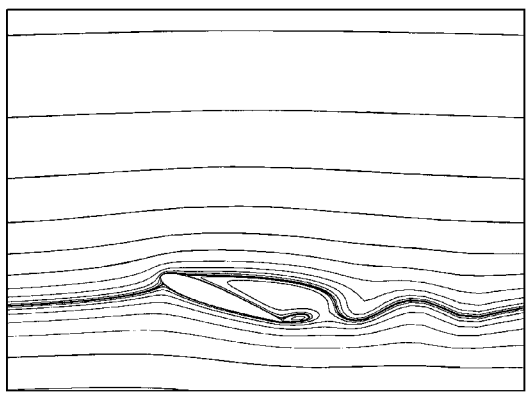

Fig. 10 Streamline plot of flow past a NACA 0015 airfoil at $Re=1.5\times10^6$ and 20-deg incidence.

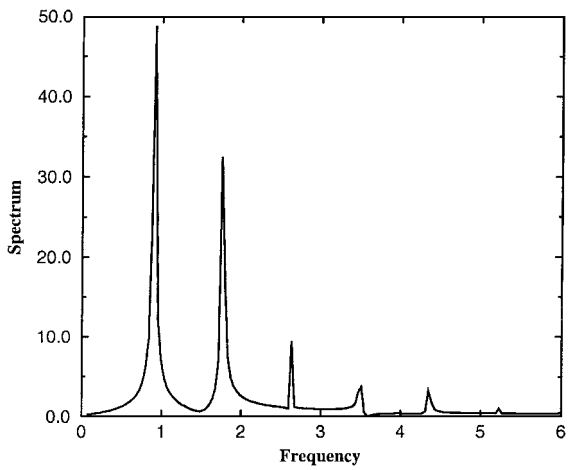

Fig. 11 Spectrum of the incompressible vorticity signal for turbulent flow past a NACA 0015 airfoil at $Re=1.5\times10^6$ and 20-deg incidence.

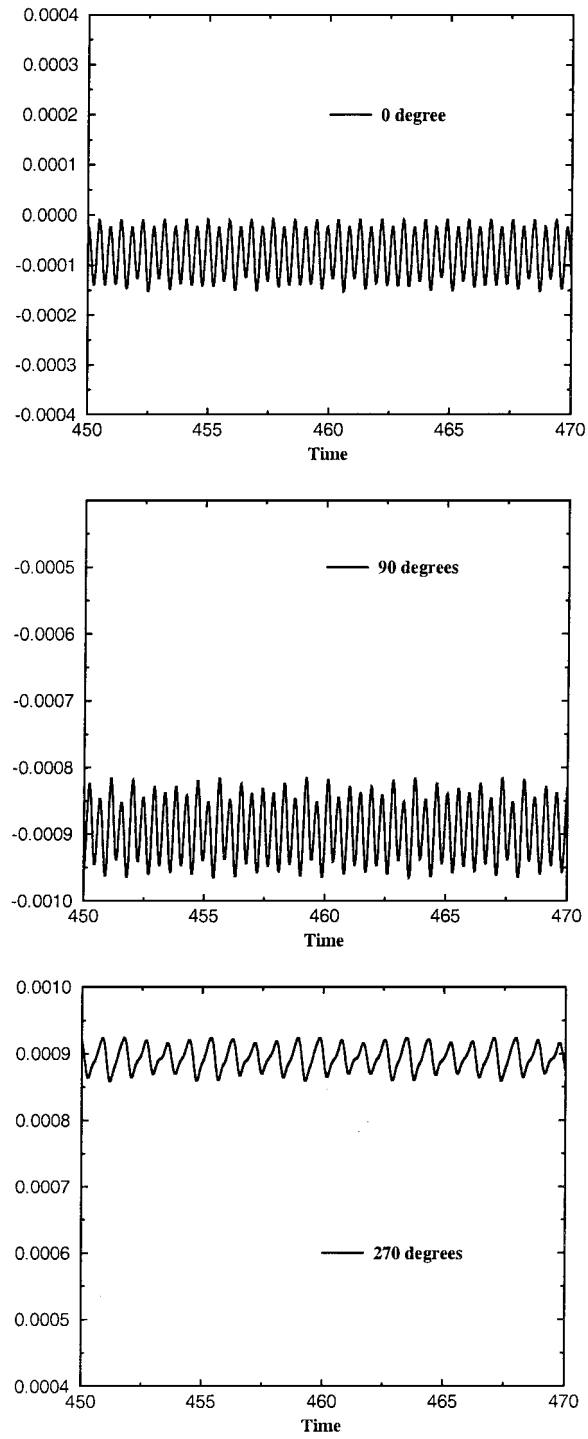

Fig. 12 Normalized Reynolds-averaged pressure $(\bar{p}-p_0)/p_0$ at $r=12$ for turbulent flow past a NACA 0015 airfoil at $Re=1.5\times10^6$, 20-deg incidence, and $M=0.2$, measured at three points around the airfoil.

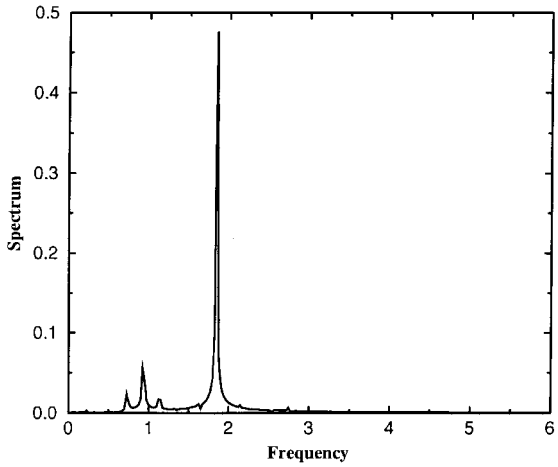

Fig. 13 Spectrum of the Reynolds-averaged pressure $(\bar{p} - p_0)/p_0$ signal for turbulent flow past a NACA 0015 airfoil at $Re = 1.5 \times 10^6$, 20-deg incidence, and $M = 0.2$.

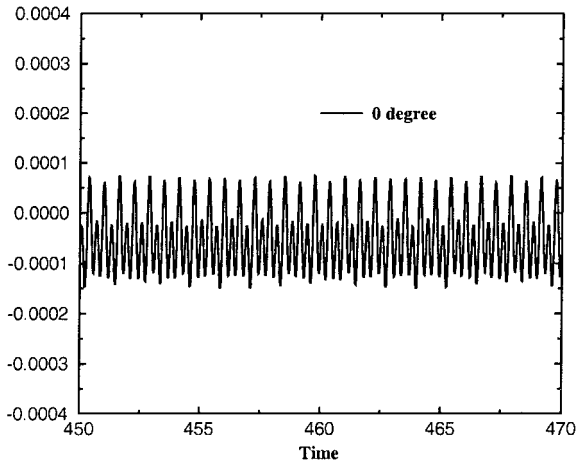

Fig. 14 Normalized Reynolds-averaged pressure $(\bar{p} - p_0)/p_0$ at $r = 12$ upstream of the airfoil for turbulent flow past a NACA 0015 airfoil at $Re = 1.5 \times 10^6$, 20-deg incidence, and $M = 0.2$, computed with 201×81 mesh.

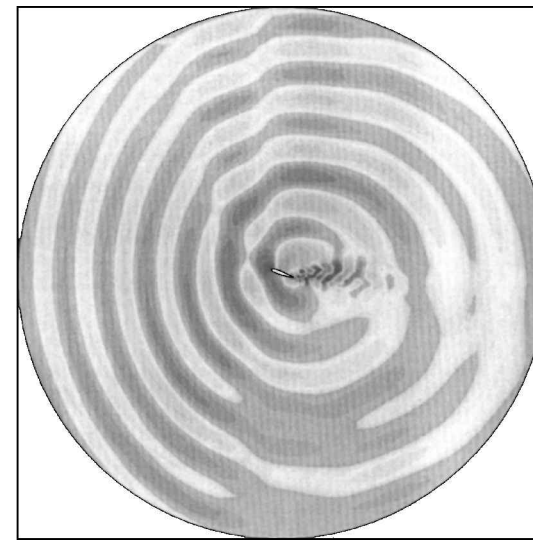

Fig. 15 Instantaneous plot of fluctuating pressure, $\bar{p} - \tilde{p}$, for turbulent flow past a NACA 0015 airfoil at $Re = 1.5 \times 10^6$, 20-deg incidence, $M = 0.2$ and $t = 420$.

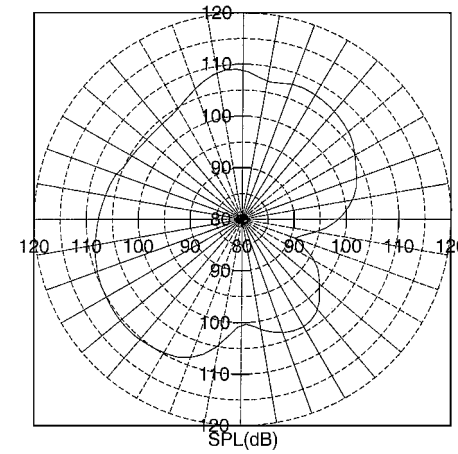

Fig. 16 Directivity pattern of NACA 0015 airfoil noise radiation at $Re = 1.5 \times 10^6$, 20-deg incidence, $M = 0.2$ and $r = 12$.

appear at nearly the same position, but the extent and amplitudes of the wake structure are smaller for the turbulent flow, corresponding to a smaller force fluctuation. Following a time history of the incompressible solution, the vortex shedding Strouhal frequency is determined to $f_t = 0.862$. When FFT analysis is performed of a vorticity signal measured at a point in the near wake of the airfoil, the Strouhal frequency is found to be accompanied by higher harmonics (see Fig. 11).

In Fig. 12, time histories of the normalized Reynolds-averaged pressure $(\bar{p} - p_0)/p_0$ are shown at $(x_1, x_2) = (12, 0)$, $(0, 12)$, and $(0, -12)$. The signals are dominated by the double Strouhal frequency. Carrying out an FFT analysis of the signals, we obtain the frequency spectrum shown in Fig. 13. Comparing the two spectra, we find that the acoustic signal carries the same frequencies as the incompressible signal except that the higher harmonic frequency is dominant in the acoustic signal.

To analyze the sensitivity of the grid spacing, an additional computation in which the number of points was doubled in the radial direction was carried out. The normalized Reynolds-averaged pressure at a distance $r = 12$ upstream the airfoil is plotted in Fig. 14. As compared with the one computed with the original mesh (Fig. 12), the amplitude (noise level) is slightly increased and higher harmonics are more pronounced.

In Fig. 15, the fluctuating pressure field $(\bar{p} - \tilde{p})$ is plotted at time instant $t = 420$. From Fig. 15, it is observed that there is about 16 grid points per wavelength in the normal direction. The directivity pattern of the airfoil noise radiation at $M = 0.2$, measured at a distance $r = 12$ from the airfoil center, is shown in Fig. 16. The levels range from 91 to 110 dB with a reference of 2×10^{-5} Pa. As compared with the laminar case, the noise level is found to be at the same level.

VI. Conclusions

A numerical algorithm for acoustic noise generation is extended to handle turbulent flows. The approach consists of two steps: a viscous incompressible flow part and an acoustic inviscid part. The acoustic part can be started at any time during the incompressible computation. The computing costs are similar to what is typical for incompressible calculations.

The model has been applied to two-dimensional laminar and turbulent flows past a NACA 0015 airfoil. The computations show that the generated acoustic noise is dominated by the Strouhal frequency and its harmonics. For the laminar case, results are compared with those obtained using the Lighthill[1] acoustic analogy (linearized wave equations). The comparisons show that noise levels and frequency content are in good agreement. The noise levels for the turbulent flow case are of the same order as for the corresponding laminar flow. Because of the Reynolds-averaged turbulence model used in the flow solver, only one frequency and its associated higher harmonics are seen. For capturing more frequencies, one should combine the acoustic model with LES or direct Navier–Stokes simulation.

The model can relatively straightforward be extended to treat three-dimensional flows. In the near future, it will be coupled to an actuator-line code to predict noise from wind turbines.

Acknowledgments

This work was supported by the Research Programme for Renewable Energy, EFP-99, under the Danish Energy Agency. The computer simulations were performed on the Cray C90 vector processor at the Danish Supercomputing Centre, UNI·C, Denmark, and were financed by the Danish Scientific Research Council.

References

[1]Lighthill, M. J., "On Sound Generated Aerodynamically. I: General Theory," *Proceedings of the Royal Society of London, Series A: Mathematical and Physical Sciences*, Vol. 211, 1952, pp. 564–587.

[2]Ffowcs Willams, J. E., and Hawkings, J. E., "Sound Generation by Turbulence and Surfaces in Arbitrary Motion," *Philosophical Transactions of the Royal Society of London, Series A: Mathematical and Physical Sciences*, Vol. 264, No. 1151, 1968, pp. 321–342.

[3]Lyrintzis, A. S., "Review: The Use of Kirchhoff's Method in Computational Aeroacoustics," *Journal of Fluids Engineering*, Vol. 116, No. 3, 1994, p. 665.

[4]Hardin, J. C., and Pope, D. S., "An Acoustic/Viscous Splitting Technique for Computational Aeroacoustics," *Theoretical and Computational Fluid Dynamics*, Vol. 6, No. 5–6, 1994, pp. 323–340.

[5]Shen, W. Z., and Sørensen, J. N., "Comment on the Aeroacoustic Formulation of Hardin and Pope," *AIAA Journal*, Vol. 37, No. 1, 1999, pp. 141–143.

[6]Shen, W. Z., and Sørensen, J. N., "Aeroacoustic Formulation of Low-Speed Flows," *Theoretical and Computational Fluid Dynamics*, Vol. 13, No. 4, 1999, pp. 271–289.

[7]Shen, W. Z., and Sørensen, J. N., "Quasi-3D Model for Rotating Airfoil," *Journal of Computational Physics*, Vol. 150, No. 2, 1999, pp. 518–548.

[8]Baldwin, B. S., and Barth, T. J., "A One-Equation Turbulence Transport Model for High Reynolds Number Wall-Bounded Flows," NASA TM 102847, 1990.

[9]Sørensen, J. N. (ed.) "VISCWIND Viscous Effects on Wind Turbine Blades," Tech. Univ. of Denmark, Rept. ET-AFM-9902, Lyngby, Denmark, Feb. 1999.

[10]Farassat, F., and Succi, G. P., "The Prediction of Helicopter Discrete Frequency Noise," *Vertica*, Vol. 7, No. 4, 1983, pp. 309–320.

[11]Farassat, F., and Brentner, K. S., "The Uses and Abuses of the Acoustic Analogy in Helicopter Rotor Noise Prediction," *Journal of the American Helicopter Society*, Vol. 33, No. 1, 1988, pp. 29–36.

[12]Cox, J. S., Brentner, K. S., and Rumsey, C. L., "Computation of Vortex Shedding and Radiated Sound for a Circular Cylinder: Subcritical to Transcritical Reynolds Numbers," *Theoretical and Computational Fluid Dynamics*, Vol. 12, No. 4, 1998, pp. 233–353.

P. J. Morris
Associate Editor